Laser and Particle Beams (2004), *22*, 183–188. Printed in the USA.

DOI: 10.1017/S0263034604222145

One-dimensional model for a laser-ablated slab under acceleration

J. RAMÍREZ, R. RAMIS, and J. SANZ
E.T.S.I. Aeronáuticos, Universidad Politécnica Madrid, Pl. Cardenal Cisneros, 1, 28040 Madrid, Spain

(Received 9 May 2003; Accepted 31 August 2003)

Abstract

A one-dimensional model for a laser-ablated slab under acceleration g is developed. A characteristic value g_c is found to separate two solutions: Lower g values allow sonic or subsonic flow at the critical surface; for higher g the sonic point approaches closer and closer to the slab surface. A significant reduction in the ablation pressure is found in comparison to the $g = 0$ case. A simple dependence law between the ablation pressure and the slab acceleration, from the initial value g_0 to infinity, is identified. Results compared well with fully hydrodynamic computer simulations with Multi2D code. The model has also been found a key step to produce indefinitely steady numerical solutions to study Rayleigh–Taylor instabilities in heat ablation fronts, and validate other theoretical analysis of the problem.

Keywords: Fluid Dynamics, Laser-ablation, Numerical simulation, Plasma-corona

1. INTRODUCTION

The problem of a solid being ablated by a laser light has been studied in the past from different points of view (Max *et al.*, 1980; Sanz *et al.*, 1981), mostly in the context of inertial confinement fusion studies (laser driven) and different geometries (one-dimensional [1D] to three-dimensional [3D]). Several ablative models have been proposed on which to base Rayleigh–Taylor instability analysis (Takabe *et al.*, 1983; Kull & Anisimov, 1986; Kull, 1989, 1991; Sanz, 1996), a key problem in achieving ignition of implosion targets. Here we approach the problem in a somewhat different way.

Let us consider a solid slab with initial temperature T_0 and density ρ_0 being thermally ablated by a laser. After a short transient period of time, a certain (high) temperature T_b is assumed to stabilize at a certain distance (critical surface) L from the slab surface (Fig. 1) that is now at temperature $T_a \ll T_b$ and density ρ_a. Heat conduction moves the energy from the critical surface to the slab and a (supposed) constant mass flow rate $\dot{m}$ is ablated from the slab mass M_0. The high ablation pressure P_a moves the slab with acceleration $g(t) = P_a/(M_0 - \dot{m}t)$. The process is analyzed using a reference attached to the slab surface.

Address correspondence and reprint requests to: J. Ramìrez, E.T.S.I. Aeronáuticos, Universidad Politécnica Madrid, Pl. Cardenal Cisneros, 1, 28040 Madrid, Spain. E-mail: julio@fmetsia.upm.es

2. HYDRODYNAMIC EQUATIONS

Continuity, momentum, and energy Navier–Stokes equations read as follows:

$$\partial\rho/\partial t = -\partial(\rho v)/\partial x \tag{1}$$

$$\partial(\rho v)/\partial t = -\partial(p + \rho v^2)/\partial x + \rho g \tag{2}$$

$$\partial\{\rho(e + v^2/2)\}/\partial t = \partial\{\rho v(h + v^2/2) + q\}/\partial x + \rho g v, \tag{3}$$

where the acceleration g has been included in the momentum and energy equations, and v is velocity, x is the distance from the slab surface (positive toward the incoming laser), p is pressure, e is specific energy, h is specific enthalpy, and q is the heat flux.

For simplicity, the ablated plasma will be taken as an ideal mono-atomic gas with equations of state (EOS): $p = \rho T$, $h = (5/2)T$, and $e = (3/2)T$. Also we will assume classical (Spitzer) heat flux with $q = -\bar{K}T^{5/2}\,dT/dx$.

The basic initial and boundary conditions, at any time, will be $T = T_b$ at $x = L$ and $T = T_a$ at $x = 0$. Other variables will be discussed later in consistency with above equations and assumptions to be made.

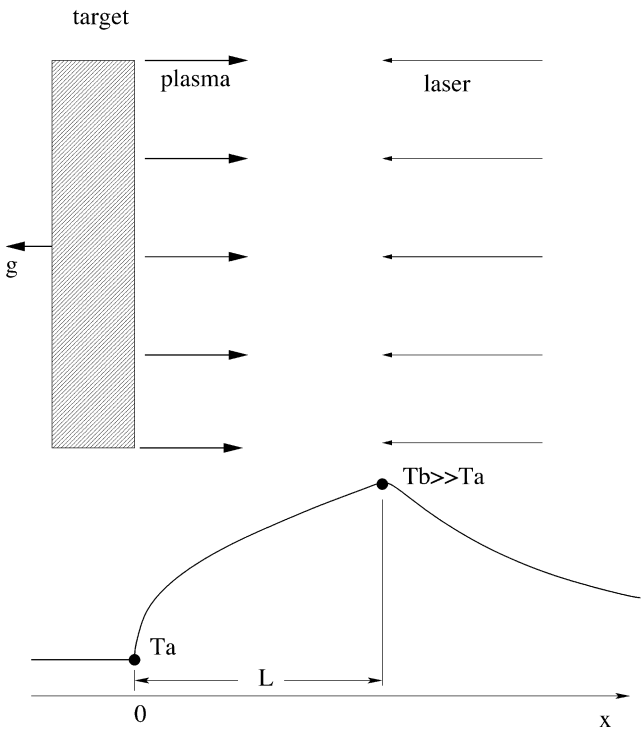

Fig. 1. A laser-ablated slab.

3. THE QUASI STEADY 1D MODEL FOR THE PLASMA CORONA

Although a real problem is not steady and requires solving fully Eqs. (1)–(3), we think a quasisteady approximation, valid on a time scale when the slab mass change is not too big, can shed some light onto the problem. Then, neglecting temporal derivatives, a constant mass flow rate $\dot{m}$ is ablated at the slab surface $x = 0$ by the energy flux coming from the right ($x > 0$ region). Integrating (1)–(3) from $x = 0$ we have

$$\rho v = \dot{m} = \rho_a v_a = \rho_b v_b \tag{4}$$

$$\dot{m}(v - v_a) + p - \int_0^x \rho g dx = P_a \quad \text{(the ablation pressure)} \tag{5}$$

$$\dot{m}(h + v^2/2 - gx) + q = const., \tag{6}$$

where, in consistency with the previous assumption $T_a \ll T_b$, we will put $T_a = v_a = 0$, and then *const.* $= 0$, as a convenient first approximation in our model.

The exact solution to the *complete model* in Eqs. (4)–(6) is discussed later in Appendix B; briefly, the eigenvalues P_a and $\dot{m}$ get determined, as functions of the boundary conditions and profiles of the different variables, only when the complete solution of the problem has been obtained. As we will confirm later, a good approximation appears, in a *simplified model*, neglecting velocity and gravity terms $v^2/2 - gx \ll h$ in (6); then, we have

$$x/L = (T/T_b)^{5/2} \tag{7}$$

with $\dot{m} = (2/5)^2 \bar{K} T_b^{5/2}/L$ for the temperature profile and the eigenvalue mass flow for all g values in terms of physical quantities.

Using dimensionless variables $x' = x/L$, $T' = T/T_b$, $v' = v/T_b^{1/2}$, and the EOS we have for the momentum equation

$$v' + T'/v' - Z\int_0^{x'} dx'/v' = R \tag{8}$$

with $Z = gL/T_b$ and $R = P_a/(\dot{m}T_b^{1/2})$ the normalized gravity acceleration and the normalized ablation pressure, respectively.

In the case of no gravity, $g = 0$, and assuming sonic flow in $x = L$, we have the solution $T' = x'^{(2/5)}$, and $v' = 1 - (1 - T')^{1/2}$, where T' and v' grow from zero in $x' = 0$, to sonic conditions $v'^2 = T' = 1$ in $x' = 1$, included in Figure 2. The eigenvalue ablation pressure is now $P_a = 2\dot{m}T_b^{1/2}$. Solution with subsonic conditions in $x' = 1$ are also possible; then, the ablation pressure increases to $P_a = (M_b + 1/M_b)\dot{m}T_b^{1/2}$ with $M_b = v_b/T_b^{1/2} \le 1$, the Mach number at $x = L$. Continuous solutions, supersonic in $x' = 1$, are not allowed in this case.

For every nonzero value of the gravity g, Eq. (8) admits phase variables η, ξ discussed in Appendix A. Here, we summarize the results. For every Z, a singular (saddle) sonic point $(x'_s, v'_s) = ((0.4/Z)^{5/3}, (0.4/Z)^{1/3})$ permits crossing from subsonic conditions, near $x = 0$, to supersonic ones, far from the origin, traveling along the integral line $v'(x')$ that links the origin with the saddle point.

For a certain characteristic value $Z_c = g_c L/T_b = \frac{2}{5}$ (the inverse number of the exponent in the Spitzer law), the saddle locates exactly at $x' = 1$, where sonic conditions are allowed (point B in Fig. A1 in Appendix A). The eigenvalue ablation pressure is now $P_a = 2\dot{m}T_b^{1/2}(1 - 0.2I_{Z=2/5}(1))$, being $I_{Z=2/5}(1) = \int_0^1 dx'/v' = 1.8100\ldots$, a numerical value

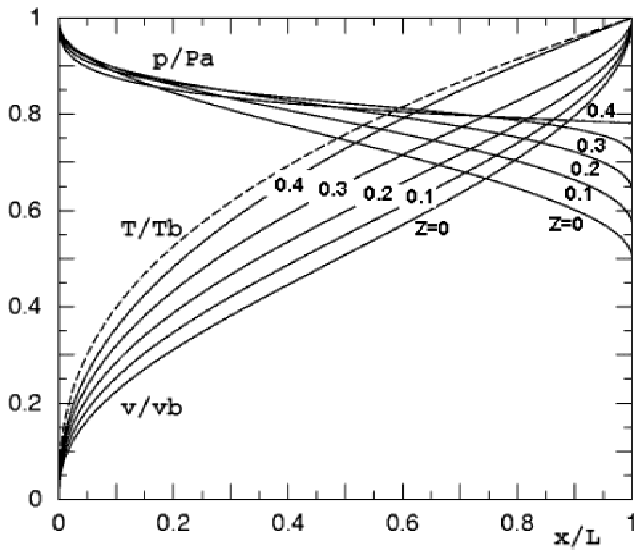

Fig. 2. Pressure, temperature, and velocity profiles for $Z \le 0.4$ (note P_a is Z dependent).

https://doi.org/10.1017/S0263034604222145 Published online by Cambridge University Press

Table 1. *The integral* $\int_0^1 dx'/v'$ *in Eq. (8) for some Z values (simplified model)*

	Z				
	0.0	0.1	0.2	0.3	0.4
$I(1)$	2.648	2.404	2.193	1.988	1.810

that appears (see Table 1) after integrating along the above mentioned integral line (note the ablation pressure is reduced about 36% in comparison with the $g = 0$ case).

For $0 < Z < \frac{2}{5}$ (*low* Z), the saddle point locates at $x_s' > 1$ (point A in Fig. A1; note that Z approaching zero gives x_s' going to infinity, and then $\eta_s = 1/x_s' < 1$). Both sonic or subsonic conditions are possible now in $x' = 1$; we are only interested in the sonic case. The solution for (8) can easily be obtained through an iterative process, if we start with the solution for $g = 0$ (with $R_0 = 2$) and use the recursive formula $v_{i+1}' = A_i - (A_i^2 - x'^{(2/5)})^{1/2}$, and new variable $A_i = 1 - 0.5Z(I_i(1) - I_i(x'))$, with $I_i(x') = \int_0^{x'} dx'/v_i'$ and $A_0 = 1$. The numerical convergence of the iterations is fast (three or four cycles are enough to get a stable graphical result; the use of absolute value inside the square root may be convenient through the calculations, and it does not influence the final true solution). The eigenvalue ablation pressure is, in this case $P_a = 2\dot{m}T_b^{1/2}(1 - 0.5ZI(1))$ where $I(1)$ is a function tabulated in Table 1 for some Z values.

For $Z > \frac{2}{5}$ (*high* Z) the saddle sonic point locates at $x_s' < 1$ (i.e., $\eta_s = 1/x_s' > 1$, point C in Fig. A1). In $x' = 1$ only certain supersonic conditions are allowed (the ones given by the mentioned integral line at that position), and the ablation pressure is now $P_a = 2\dot{m}T_b^{1/2}(0.4/Z)^{1/3}(1 - 0.2I_{Z=2/5}(1))$ where the factor $(0.4/Z)^{1/3}$ can also be read as v_s', or $T_s'^{1/2}$, or $x_s'^{1/5}$ (note that Z approaching infinity gives P_a going to zero).

In Figure 2, the corresponding profiles for pressure, temperature, and velocity are given for some Z values (0, 0.1, 0.2, 0.3, and 0.4). Also, in Figure 3, we show the normalized ablation pressure R as a function of the normalized gravity acceleration Z for a moderate range of Z values.

4. THE NONSTEADY EVOLUTION OF THE SLAB

At every instant time, the slab mass $M = M_0 - \dot{m}t$ is accelerated by the ablation pressure $P_a = R(Z)\dot{m}T_b^{1/2}$ and this allows us, in a first approximation, to couple the corona model and the slab evolution in a consistent manner. In terms of a characteristic burning time $t_b = M_0/\dot{m}$ with $\dot{m}$ from (7) and a characteristic fluid time $t_c = L/T_b^{1/2}$, we found the simple expression

$$t/t_c = t_b/t_c - R(Z)/Z. \tag{9}$$

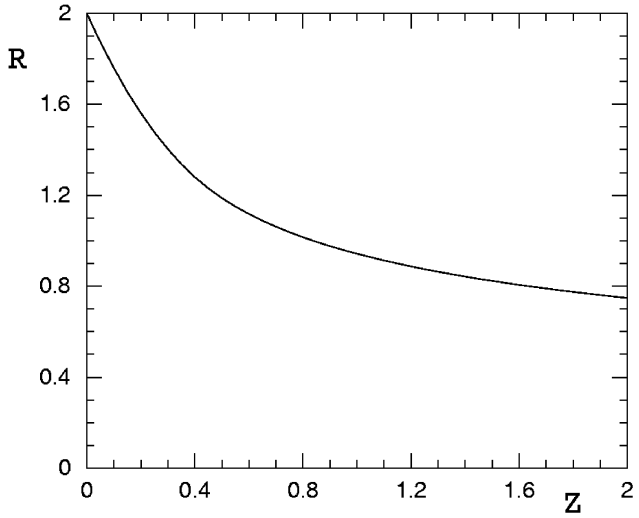

Fig. 3. Normalized ablation pressure R versus normalized acceleration Z.

At $t = 0$ we have $(R(Z)/Z)_0 = t_b/t_c$. In Figure 4, it is given $R(Z)/Z$, nearly a straight line in logarithmic scale, for a wide range of Z values. For every practical case (given T_b, L, $\bar{K}$, and M_0), entering with t_b/t_c in the vertical axis, we can read the normalized initial acceleration Z_0 in the horizontal one.

Although Eq. (9) and Figure 4 provide a useful tool to evaluate the function $Z(t)$, taking into account that for $Z > 0.4$ is $R/Z = const./Z^{4/3}$ and Z necessarily increases with time, for practical purposes, we propose the simple analytical formula

$$Z = Z_0/(1 - (t/t_c)/(R/Z)_0)^{3/4} \tag{10}$$

for the normalized slab acceleration due to the ablation pressure.

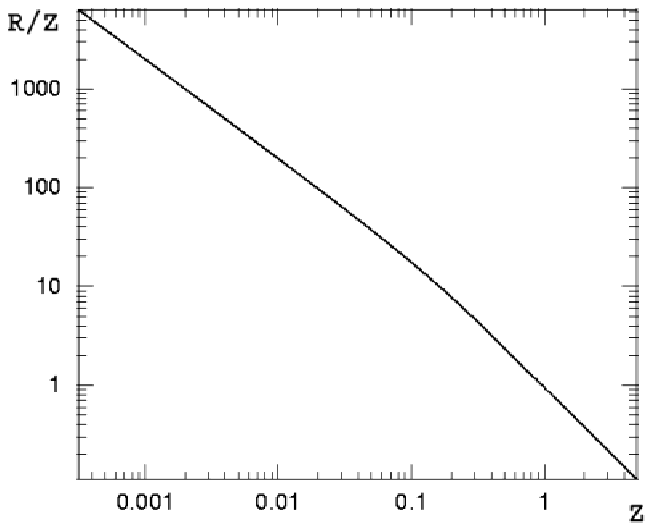

Fig. 4. The $R(Z)/Z$ function.

https://doi.org/10.1017/S0263034604222145 Published online by Cambridge University Press

5. THE MODEL AND THE NUMERICAL SIMULATION

Two kinds of problems have been studied numerically, using computer code Multi2D (Ramis & Meyer-ter-Vehn, 1992), to test and validate the above simplified model. First, a plane target with initial velocity V_0 is decelerated by a laser until the target is completely ablated. Typically, we have used T_a/T_b around $\frac{1}{40}$ and an initial normalized deceleration in the range of 0.05 to 0.15. Computed temperature, velocity, and pressure profiles have been followed along the time and compared to the ones in the model. In velocity and pressure the agreement has been found good, except that numerical values for the ablation pressure P_a are typically around 90% the ones provided in the model. The neglecting of the velocity and gravity terms in the energy equation (6), to solve the model in Section 3, has been found responsible for half of this disagreement. The other part may be due to the fact that numerical simulations are really nonsteady whereas the model is quasi-steady and, obviously, they must show differences. Regarding the temperature profiles, the fitting has been found very good.

Second, both the simplified and the complete models for the plasma region $x > x_a$, besides the isentropic approximation with g nonzero ($v = v_a(T_a/T)^{3/2}$, $T = T_a + 0.4Z(x - x_a)$) for the slab region $x < x_a$, up to a position where profiles get multivalued (Mach number $(5/3)^{1/2}$), have been used as initial solution to build "indefinitely steady numerical profiles" on which to study numerically the evolution of fundamental Rayleigh–Taylor instability problems in ablation fronts (Sanz *et al.*, 2002; including single and multimode evolution in 2D and 3D axisymmetrical geometries, cutoff wave length determination, etc.) in a wide range of values for the parameters T_a/T_b and Z. No special advantage has been found in using the complete model instead of the simplified one. Results of these studies will be published shortly, elsewhere.

6. CONCLUSIONS

From fundamental laws we have developed a 1D model for a laser-ablated slab under acceleration g. The assumption of a quasisteady problem, although strictly valid only for short periods of time or low mass ablation rates, has been found useful to close the nonsteady problem. A simple law for the acceleration $g(t)$ of the nonsteady laser-ablated slab is proposed. In the quasisteady approximation, a characteristic acceleration g_c is identified; above this value, a sonic point appears between the slab and the critical surface; the ablation pressure is strongly reduced $\propto 1/g^{1/3}$. The hydrodynamic profiles in the simplified model have been proved a key step in the numerical analysis of basic Rayleigh–Taylor instability problems in ablation fronts.

ACKNOWLEDGMENTS

This research was supported by the CICYT of Spain (C97010502, FTN 2000-2048-C0301), and by the EURATOM/CIEMAT association in the framework of the "IFE Keep-in-Touch Activities."

REFERENCES

Kull, H.J. (1989). Incompressible description of Rayleigh-Taylor instabilities in laser-ablated plasmas. *Phys. Fluids B* **1**, 170–182.

Kull, H.J. (1991). Theory of the Rayleigh-Taylor instability. *Phys. Rep.* **206**, 197–325.

Kull, H.J. & Anisimov, S.I. (1986). Ablative stabilization in the incompressible Rayleigh-Taylor instability. *Phys. Fluids* **29**, 2067–2075.

Max, C.E., McKee, C.F. & Mead, W.C. (1980). A model for laser-driven ablative implosions. *Phys. Fluids* **23**, 1620–1645.

Ramis, R. & Meyer-ter-Vehn, J. (1992). A computer code for two-dimensional radiation hydrodynamics, Report MPQ-174. Max-Planck Institute für Quantenoptik. Garching, Germany.

Sanz, J. (1996). Self-consistent analytical model of the Rayleigh-Taylor instability in inertial confinement fusion. *Phys. Rev. E* **53**, 4026–4045.

Sanz, J., Linan, A., Rodriguez, M. & Sanmartìn, J.R. (1981). Quasi-steady expansion of plasmas ablated from laser-irradiated pellets. *Phys. Fluids* **24**, 2098–2106.

Sanz, J., Ramirez, J., Ramis, R., Betti, R. & Town, R.P.J. (2002). Nonlinear theory of the ablative Rayleigh-Taylor instability. *Phys. Rev. Lett.* **89**, 195002-1–195002-4.

Takabe, H., Montierth, L. & Morse, R.L. (1983). Self-consistent eigenvalue analysis of Rayleigh-Taylor instability in an ablating plasma. *Phys. Fluids* **26**, 2299–2307.

APPENDIX A: THE PHASE PLANE IN THE SIMPLIFIED MODEL

The complete discussion of the solutions in Eqs. (7)–(8) appears analyzing the corresponding phase plane. Using (7) in (8) and after derivation we have

$$dv'/dx' = v'(Z - 0.4/x'^{(3/5)})/(v'^2 - x'^{(2/5)}) \qquad \text{(A.1)}$$

that shows, in the physical plane (x', v') a singular (node) critical point at the origin (0,0), a singular (saddle) critical point at $(x'_s, v'_s) = ((0.4/Z)^{5/3}, (0.4/Z)^{1/3})$, and a sonic line $v'^2 = x'^{(2/5)}$ (with $T' = x'^{(2/5)}$) where the Mach number is unity. Normalizing position and velocity with corresponding values at this saddle point we have, for the new phase variables $\eta = x'/x'_s$ and $\xi = v'/v'_s$, the normalized equation

$$d\xi/d\eta = 0.4\xi(1 - 1/\eta^{3/5})/(\xi^2 - \eta^{2/5}), \qquad \text{(A.2)}$$

with the singular points at (0,0) and (1,1), and the sonic line $(\xi = \eta^{1/5})$, all of them represented in Figure A1; also some integral lines coming from the node and others approaching the saddle are drawn.

The characteristic value $Z_c = 0.4$ (i.e., $g = 0.4T_b/L$) plays an important role in the solutions of Eq. (A1). For $Z = Z_c$, both the physical (x', v') and the normalized (η, ξ) phase

https://doi.org/10.1017/S0263034604222145 Published online by Cambridge University Press

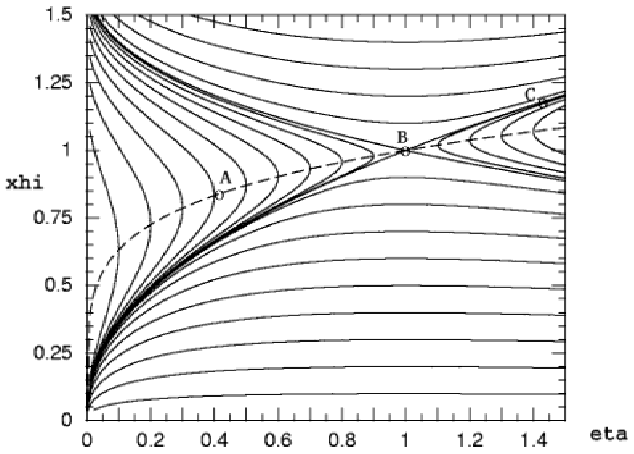

Fig. A1. The normalized phase plane (η, ξ) (dashed, the sonic line).

planes are identical; only one integral line is allowed to go continuously from the origin $x' = 0$ to sonic conditions in $x' = 1$ (point B in Fig. A1); supersonic conditions are not possible there. For $Z > 0.4$ (high g) $x'_s < 1$ (thus $\eta_b = 1/x'_s > 1$, point C in Fig. A1) and only specific supersonic conditions are allowed in $x' = 1$ when coming from $x' = 0$ (the ones fixed by the mentioned integral line at that point). For $Z < 0.4$ (low g) $x'_s > 1$ (thus $\eta_b = 1/x'_s < 1$, point A in Fig. A1) and only a specific sonic solution is possible in $x' = 1$ (also several subsonic ones, or supersonic multivalued, which we are not interested in).

APPENDIX B: THE COMPLETE MODEL

As we advanced in Section 3, in the case of $g = 0$, in the *simplified model*, we neglect $v^2/2 \ll h$; then the solution of Eq. (4)–(6) with $T_a = v_a = 0$ leads to

$$\dot{m} = \rho.v, \qquad (P_a/\dot{m} - v)v = T, \qquad x = (4/25)(\bar{K}/\dot{m})T^{5/2}, \tag{B.1}$$

the condition of the sonic point in $x = L$ giving eigenvalues $\dot{m} = (4/25)\bar{K}T_b^{5/2}/L$ and $P_a = 2\dot{m}T_b^{1/2}$ in terms of the physical quantities $\bar{K}$, T_b, and L.

Using dimensionless variables $x' = x/L$, $\rho' = \rho/(\dot{m}/v_b)$, $v' = v/v_b$, and $T' = T/T_b$, we have the normalized solution

$$\rho' = 1/v', \qquad v' = 1 - (1 - T')^{1/2}, \qquad T' = x'^{(2/5)},$$
$$p' = p/P_a = 1 - v'/2, \tag{B.2}$$

which is represented in Figure B1.

As we are interested here in the *complete model*, the energy equation (6) can be put in differential form $dx(1 + 0.2v^2/T - 0.4gx/T) = 0.4(\bar{K}/\dot{m})T^{3/2}\,dT$. Using the above dimensionless variables and integrating from $x' = 0$ we have

$$L(x' + 0.2J(x') - 0.4ZK(x')) = 0.16(\bar{K}T_b^{5/2}/\dot{m})T'^{(5/2)}, \tag{B.3}$$

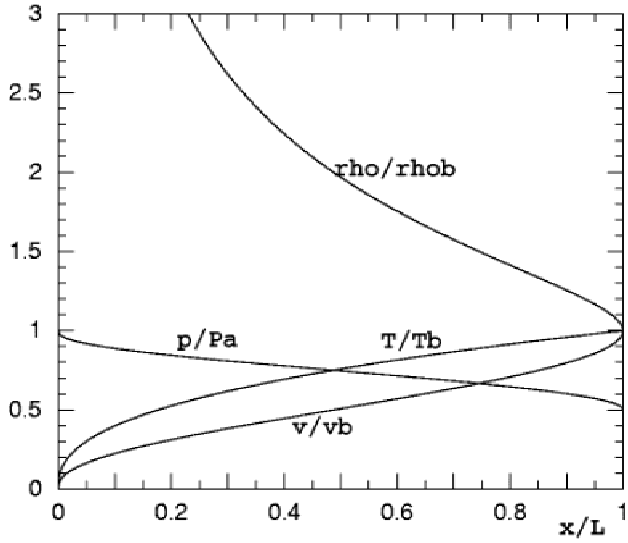

Fig. B1. The normalized profiles for $g = 0$.

with $Z = gL/T_b$, $J(x') = \int_0^{x'} dx' v'^2/T'$, and $K(x') = \int_0^{x'} dx' x'/T'$. Evaluating the above equation in $x' = 1$ gives the eigenvalue mass flow

$$\dot{m} = 0.16\bar{K}T_b^{5/2}/(L[1 + 0.2J(1) - 0.4ZK(1)]). \tag{B.4}$$

In the same manner, the dimensionless momentum equation is

$$[P_a/(\dot{m}T_b^{1/2}) + ZI(x') - v']v' = T', \tag{B.5}$$

with $I(x') = \int_0^{x'} dx'/v'$, and, after evaluation in $x' = 1$, with Mach unity there for moderate Z values, we have the other eigenvalue

$$P_a = 2\dot{m}T_b^{1/2}[1 - 0.5ZI(1)]. \tag{B.6}$$

The quantities $I(1)$, $J(1)$, and $K(1)$ for every Z appear after the complete integration of the problem has been done, and are given in Table B1 for some Z values of interest.

The complete analysis of Eqs. (B3)–(B6) leads to a phase plane similar to the one considered in Appendix A. For every Z, a (saddle) critical sonic point is found in (x'_s, v'_s) at

Table B1. *The integrals I, J, K for some Z values (complete model)*

	Z					
	0.00	0.10	0.20	0.30	0.40	0.4027
$I(1)$	2.7052	2.4469	2.2061	2.0034	1.8056	1.8050
$J(1)$	0.3623	0.4094	0.4701	0.5490	0.6620	0.6624
$K(1)$	0.6312	0.6298	0.6285	0.6267	0.6259	0.6260

https://doi.org/10.1017/S0263034604222145 Published online by Cambridge University Press

the x'_s value that is solution of the equation $dT'/dx' = Z$ and is numerically obtained after integrating the solution $T'(x')$. We have found that for a certain characteristic value $Z_c = 0.4027\ldots$ $x'_s = 1$.

For Z below this Z_c value, sonic solutions in $x' = 1$ are possible, and can be obtained as follows: Using (B4) and (B6) in (B3) and (B5), we have

$$T'^{(5/2)} = [x' + 0.2J(x') - 0.4ZK(x')]/ \times [1 + 0.2J(1) - 0.4ZK(1)] \quad \text{(B.7)}$$

$$v'_1 = B - (B^2 - T')^{1/2}, \quad \text{(B.8)}$$

with $B = 1 - 0.5Z[I(1) - I(x')]$, which can be solved numerically. Starting with the universal solution (B2) $T'_0 = x'^{0.4}$, $v'_0 = 1 - (1 - T'_0)^{1/2}$, we evaluate the integrals I, J, K, and the auxiliary variable B; with (B7) we get T'_1 and with (B8) also v'_1 and so on for the following steps (three or four cycles are enough for good graphical results). In Figure B2 we show the obtained v' profiles for some Z values; to compare, dashed lines show the corresponding ones using the simplified model described in Section 3. We see that the simplified model represents quite well the complete one.

For Z above Z_c, the saddle sonic point x'_s moves toward the origin (and this distance becomes the convenient normalizer, instead of L, for the subsonic part of the plasma region).

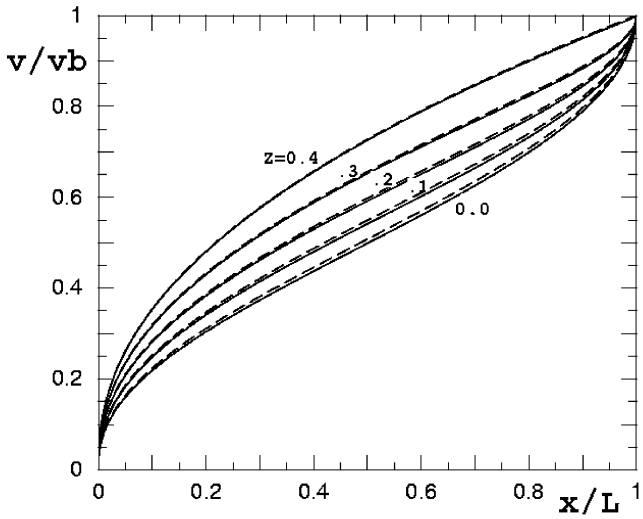

Fig. B2. Velocity profiles for some Z values in the complete model (dashed lines represent the simplified one).

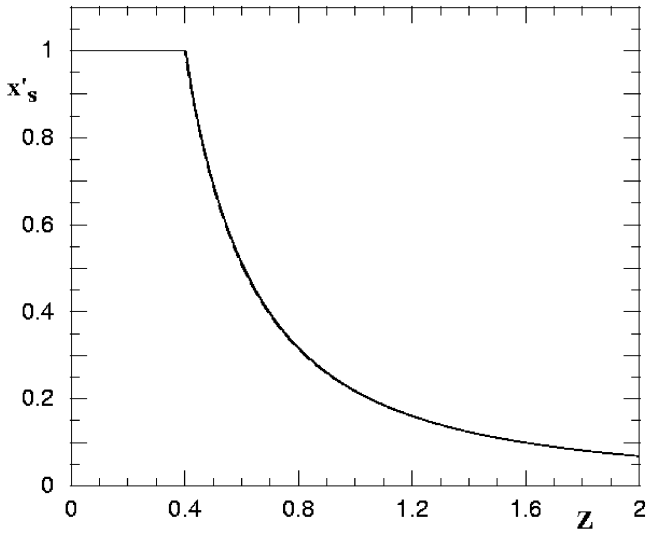

Fig. B3. Sonic point location versus acceleration (dashed line represents the simplified model).

Figure B3 shows x'_s as function of Z (dashed line represents the simplified model). We also see both models fit quite well.

Finally Figure B4 compares both models as far as both eigenvalues, the ablation pressure, and the mass flow is concerned. Typically, the complete model proposes around 6–8% less flow mass and more ablation pressure.

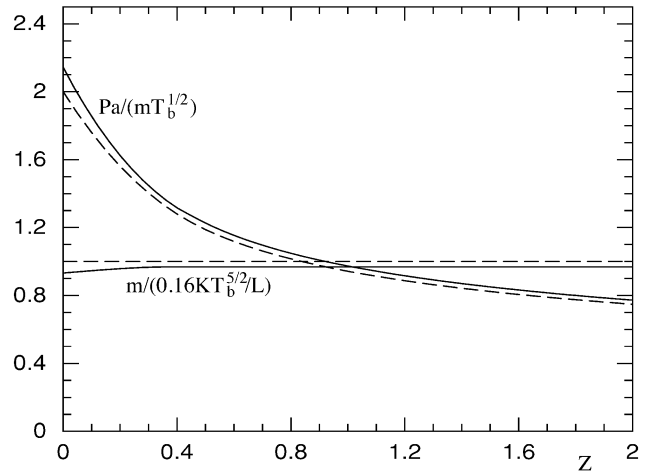

Fig. B4. Ablation pressure and mass flow versus acceleration (dashed lines represent the simplified model).

https://doi.org/10.1017/S0263034604222145 Published online by Cambridge University Press